Electronic supplementary information (ESI)

SO_2-Tolerant Catalytic Reduction of NO_x via Confining Active Species in TiO_2 Nanotubes

Ziqiang Xu, [a] Sarawoot Impeng, [b] Xinyu Jia, [a] Fuli Wang, [a] Yongjie Shen, [a] Penglu Wang, [a,*] and Dengsong Zhang [a,*]

[a] International Joint Laboratory of Catalytic Chemistry, Department of Chemistry, College of Sciences, Shanghai University, Shanghai 200444, P. R. China.

[b] National Nanotechnology Center, National Science and Technology Development Agency, Pathum Thani, 12120, Thailand.

*E-mail: dszhang@shu.edu.cn; plwang@shu.edu.cn.

The Supporting Information includes 47 Pages, 29 Figures and 6 Tables.

Table of Contents

Synthesis of Catalysts

Synthesis of TiO_2 nanotubes (NTs): The preparation of TiO_2 NTs was completed by a typical hydrothermal method. 2 g P25 powder and 70 mL of 10 mol/L NaOH solution were added into a Teflon autoclave and stirred for 6 h. After mixing evenly, the autoclave was placed into the oven at 130 ºC for 24 h to conduct the hydrothermal reaction. After the hydrothermal reaction was completed, the transparent liquid in the upper layer of autoclaves was poured out. The white precipitation in the under layer was collected and washed with 0.1 mol/L HCl solution to ensure the pH of suspension solution equal to 1.6. At this point, the original large granular sediment gradually changed into fine particles. The suspension was then washed several times with deionized water until its pH was equal to 7. The excess aqueous solution was poured out and the white sediment was soaked into anhydrous ethanol at room temperature for 24 h. After the ethanol treatment was completed, the sediment was filtered, dried in an oven at 80 ºC to obtain the TiO_2 NTs.

Synthesis of CuO-out-TiO_2 NTs: To study the confinement effect on the SCR performance and SO_2 tolerance with CuO-TiO_2 NTs, the CuO-out-TiO_2 NTs was synthesized. In details, 0.5 g ethanol treated TiO_2 NTs was immerged in superfluous xylene for 12 h to packing the tubular channels, followed by the addition of aqueous solution with 0.0756 g $Cu(NO_3)_2 \cdot 3H_2O$ dissolved. Then a solution of NH_4HCO_3 dissolved in aqueous ammonia (26-28%) was added to facilitate the extraction of NTs from xylene into the aqueous phase. After stirring for 6 h, a standing and layering

process for the solutions was followed. Then, the mixture was evaporated at 80 ºC under stirring for 1 h. Subsequently, the mixture was centrifuged, washed (at least 3 times with deionized water), dried in an oven at 80 ℃ for 12 h, and calcined in a muffle furnace at 400 ºC for 4 h in static air with a heating rate of 2 ºC/min. The catalyst was designated as CuO-out-TiO_2 NTs for copper oxides supported outside TiO_2 NTs.

Catalysts Characterization

The microstructure of the catalyst was observed using a transmission electron microscope (TEM, JEM-200CX) and a high-resolution transmission electron microscope (HRTEM, JEM-2100F). The X-ray Diffraction (XRD) diffraction pattern was obtained by X-ray diffractometer (3KW D/MAX2200V PC, Japan) with Cu Kα (40 kV, 40 mA) radiation in the 2θ range of 10° to 90° with a scan rate of 8°/min. The Raman spectra of catalysts was obtained by using Raman spectrometer (LabRAM HR Evolution, Horiba, France) with the laser at 532 nm as the excitation source. The UV-vis diffuse reflectance (UV-vis) spectra were recorded by the UV-vis spectrophotometer (UV-vis absorbance, Cary5000, 229 Agilent, USA). Additionally, $BaSO_4$ was used as a reference in the range of 200~900 nm at room temperature. X-ray photoelectron spectroscopy (XPS) system equipped with Al Kα radiation (PHI-5300) could be applied to research the surface atomic valence of catalysts. and the binding energy was calibrated by the containment carbon peak (C 1s = 284.8 eV). The microstructure and element distributionof the catalyst was observed by HRTEM-EDX (JEOL JEM-2100F) at 200 kV. The chemical composition and atomic proportion of the materials were measured by Agilent 7700 inductively coupled plasma-atomic emission spectrometry (ICP-AES). Nitrogen adsorption–desorption tests were measured at 77 K by a nitrogen adsorption instrument (U.S. Quanta chrome ASAP 2020M), and the specific surface area was calculated by the Brunaue-Emmett-Teller (BET) method. The impurities adsorbed on the catalyst was removed by vacuum degassing effectively at 200 °C for

10 h before the BET tests. The redox performances of catalysts were obtained by the hydrogen temperature-programmed Reduction (H_2-TPR) which was conducted on a Micromeritics AutoChem 2950 II auto-adsorption apparatus with a thermal conductivity detector (TCD). Previously, 80 mg of each catalyst was treated under Ar atmosphere with a flow rate of 30 ml/min at 300 ºC for 30 min, then cooled to room temperature under Ar atmosphere. Afterwards H_2-TPR program runed in which the catalysts were exposed to 10 % H_2/Ar and the reactor temperature raised from room temperature to 900 ºC with a rate of 10 ºC/min. The Micromeritics AutoChem 2920 II auto-adsorption apparatus was employed for NH_3 temperature-programmed desorption experiments (NH_3-TPD) with a TCD and Mass spectrometer (OMNISTAR) to monitor the NH_3. Similarly, before the NH_3-TPD experiments, 80 mg of catalysts were outgassed under He protection (30 ml/min) at 300 ℃ for 30 min and then cooled to 100 ℃. Then, samples were exposed to 4% NH_3/He for 1h at 100 ºC, followed by purging for 1 h with He to remove the physically adsorbed NH_3. Finally, the temperature was raised to 900 ºC with a ramping rate of 10 ºC/min. The Tianjin XQ TP-5080 auto-adsorption apparatus equipped with a TCD monitor and Mass spectrometer (OMNISTAR) was employed for performing SO_2 + O_2 temperature-programmed desorption mass spectra experiments (SO_2 + O_2-TPD-MS). Prior to the TPD experiments, 80 mg of catalysts were treated under He protection (30 mL/min) at 300 °C for 30 min, then cooled to 100 °C. Samples were exposed to 500 ppm SO_2 + 5% O_2/N_2 for 1h at 30 °C, and purged by N_2 for 1 h at the same temperature. Finally, the

temperature was raised to 900 °C with a ramping rate of 10 °C/min. And the Tianjin XQ TP-5080 auto-adsorption equipped with a TCD monitor and Mass spectrometer (OMNISTAR) was also used for performing temperature-programmed decomposition (TPDC) experiments. Prior to the TPDC experiments, 80 mg of sulfated catalysts were treated under He protection (30 mL/min) at 300 °C for 30 min, and then cooled to 100 °C. Samples were exposed to 1000 ppm NO + 5% O_2/N_2 for 1 h at 30 °C, and purged by N_2 for 1 h at the same temperature. Finally, the temperature raised to 900 °C with a ramping rate of 10 °C/min.

In situ diffuse reflectance infrared Fourier transform spectroscopy (*in situ* DRIFTS) experiments were studied on a Nicolet 6700 spectrometer with a liquid nitrogen cooled mercury cadmium telluride (MCT) detector. All DRIFTS were collected in the wavenumber range of 4000 cm^{-1} to 1000 cm^{-1} in the Kubelka-Munk format, accumulating 64 scans per minute at 4 cm^{-1} resolution. Prior to each test, each sample was pre-treated at 300 °C under N_2 flow for 0.5 h and then regulated to the target temperature to obtain a background spectrum which should be deducted from the sample spectra. Prior to collecting a sample spectrum, it was necessary to collect a background spectrum at the target temperature which needed to be deducted from the sample spectra. As for the adsorption of NH_3, NO + O_2 or SO_2 + O_2 studies, after obtaining the background spectra at different temperatures, the catalysts were exposed to a flow of 1000 ppm of NH_3, 1000 ppm NO + 5 vol% O_2 or 1000 ppm SO_2 + 5 vol% O_2 at 30 °C for 1 h. The desorption process then went on under a flow of N_2 and was

recorded at corresponding temperatures of background spectrum. Furthermore, for the transient reactions between 1000 ppm NO + 5 vol% O_2 (NH_3) and pre-adsorbed 1000 ppm NH_3 (or NO + O_2), after the same pretreatment, the catalysts were exposed to NH_3 (or NO + O_2) for the adsorption. One hour later, the samples were switched to a flow of NO + O_2 (or NH_3) and meanwhile the reaction process was recorded as a function of time. For the transient reactions between 1000 ppm NO +100 ppm SO_2 + 5 vol% O_2 (NH_3) and pre-adsorbed 1000 ppm NH_3 (or NO + SO_2 + O_2), after the same pretreatment, the catalysts were exposed to NH_3 (NO + SO_2 + O_2) for the adsorption. One hour later, the samples were switched to a flow of NO + SO_2 + O_2 (or NH_3) and meanwhile the reaction process was recorded as a function of time.

DFT calculations

To better understand the interaction between metal oxide catalysts and TiO_2 supports, periodic DFT calculations were performed with the Vienna *ab initio* simulation package (VASP). [1] The projector-augmented wave pseudopotentials [2] were used for the electrons-nucleus interactions, whereas the generalized gradient approximation (GGA) with the Perdew-Burke-Ernzerhof (PBE) functional was employed for the exchange-correlation of electrons. [3] An energy cutoff of 400 eV was selected for the plane wave basis. The van der Waals interaction was corrected using the DFT-D3 method of Grimme *et al*.[4] We set the k-point of the Brillouin zone to 3 × 3 × 1 for all calculations. [5] Based on Dudarev's approach, [6] the Hubbard correction was applied to the Ti 3d states in which a single parameter U_{eff} was chosen to be 5.0 eV. The criterions of the electron self-consistent energy and the force convergence were 10^{-5} eV and 0.03 eV/Å, respectively.

For $Ti_3H_2O_7$ (110) surface, a unit cell of 9.47 Å × 16.35 Å × 25.62 Å containing a total of 96 atoms separated by a vacuum space of 18 Å was employed. The adsorption energy of each metal oxide catalyst (MOC) on $Ti_3H_2O_7$ (110) surface was calculated as:

$$E_{ads} = E_{MOC/surface} - (E_{MOC} + E_{surface})$$

where $E_{species/surface}$ is the total energy of MOC/surface complex. And E_{MOC} and $E_{surface}$ are the total energies of corresponding MOC and surface, respectively. The more negative value indicates the stronger interaction.

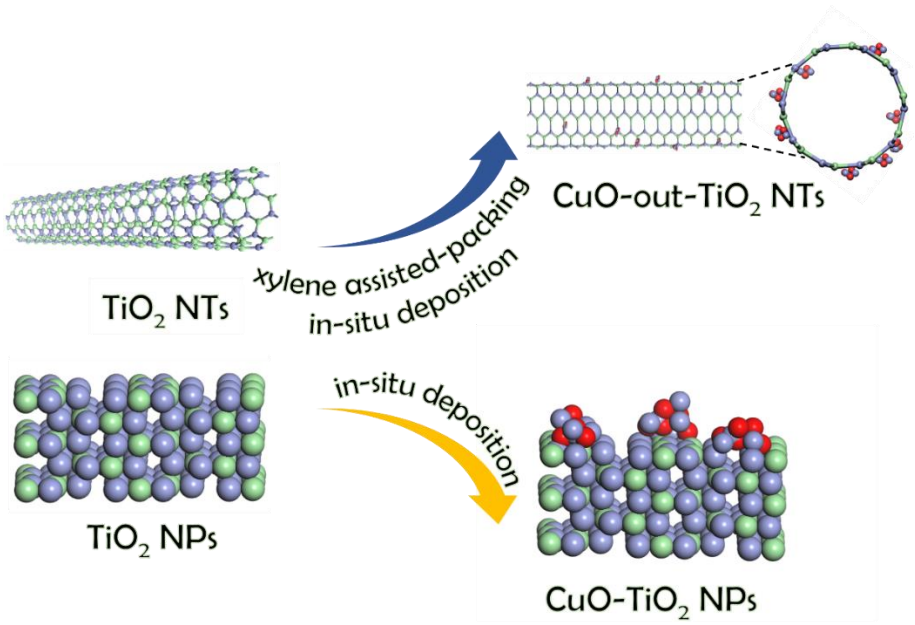

Figure S1. Schematic illustration of the synthesis procedure of CuO-TiO_2 NPs and CuO-out-TiO_2 NTs.

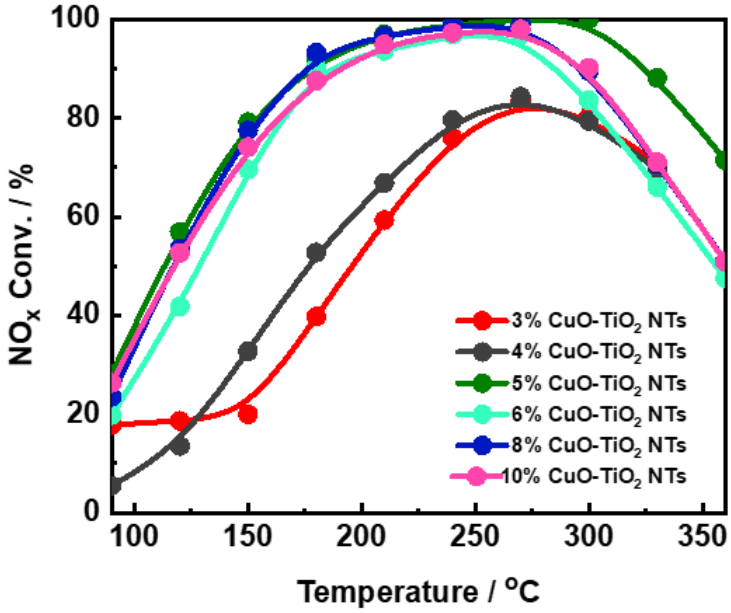

Figure S2. Plots of NO_x conversion as a function of reaction temperature over CuO-TiO_2 NTs supported with different contents of CuO. Reaction conditions: 500 ppm of NO, 500 ppm of NH_3 and 5 vol% O_2, N_2 as the balance gas, and GHSV of 50,000 h^{-1}.

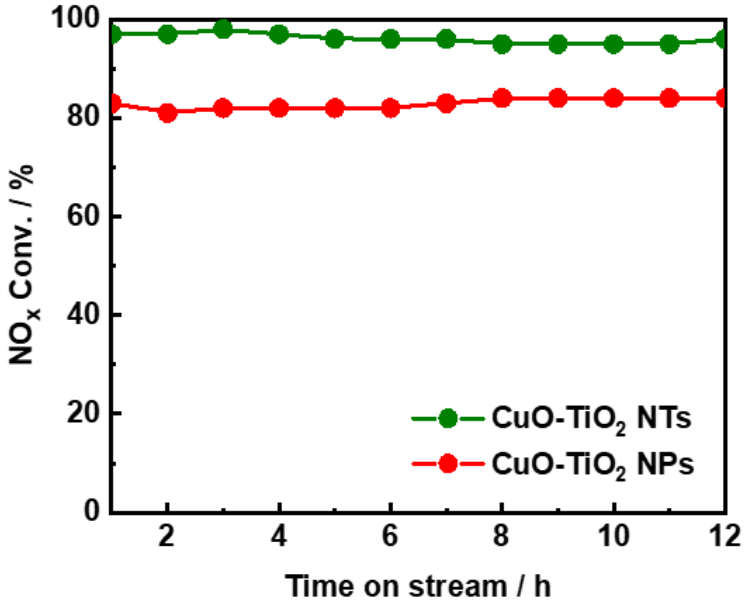

Figure S3. Plots of NO_x conversion as a function of reaction time over CuO-TiO_2 NTs and CuO-TiO_2 NPs at 270 °C. Reaction conditions: 500 ppm of NO, 500 ppm of NH_3 and 5 vol% O_2, N_2 as the balance gas, and GHSV of 50,000 h^{-1}.

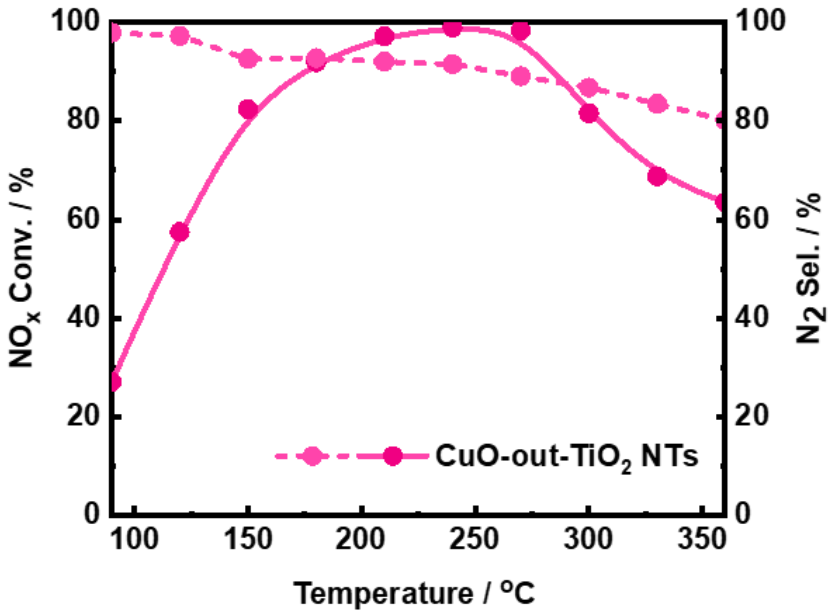

Figure S4. Plots of NO_x conversion (solid line) and N_2 selectivity (dash line) as a function of reaction temperature over CuO-out-TiO_2 NTs. Reaction conditions: 270 °C, 500 ppm of NO, 500 ppm of NH_3 and 5 vol% O_2, N_2 as the balance gas, and GHSV of 50,000 h^{-1}.

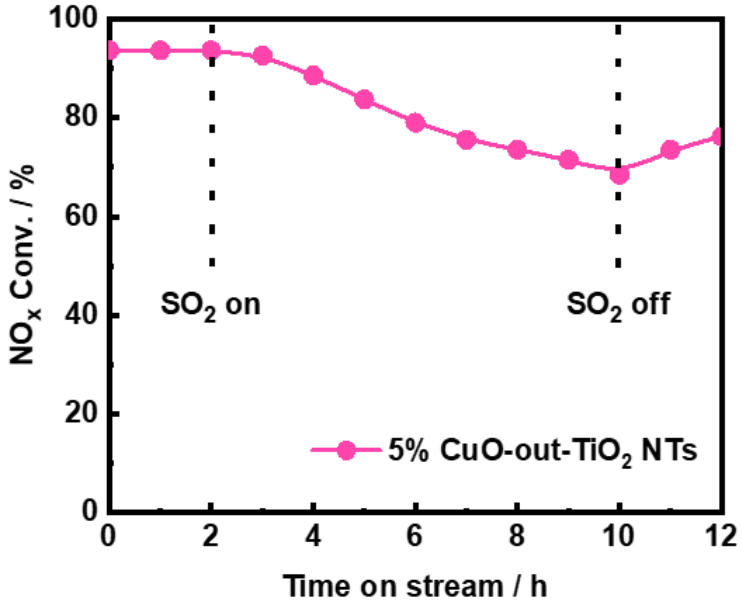

Figure S5. Plots of NO_x conversion as a function of reaction time over CuO-out-TiO_2 NTs in the presence of SO_2. Reaction conditions: 270 °C, 500 ppm of NO, 500 ppm of NH_3, 5 vol% O_2, 100 ppm of SO_2, N_2 as the balance gas, and GHSV of 50,000 h^{-1}.

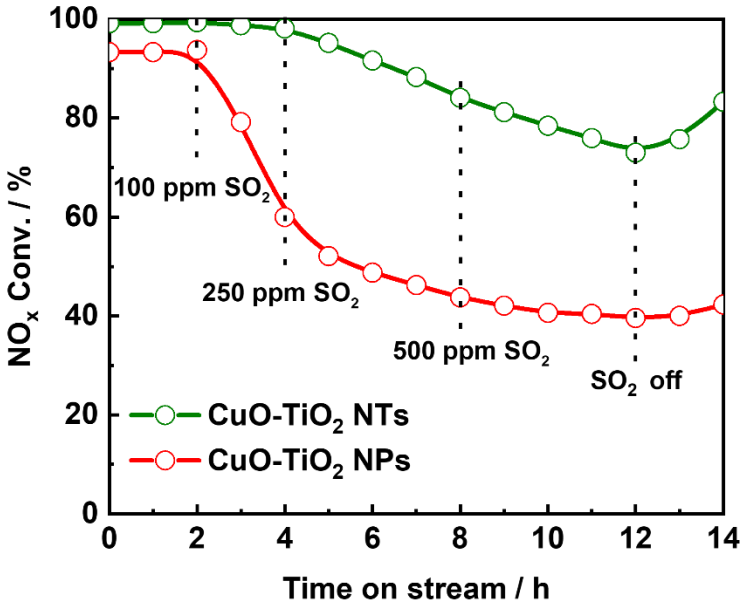

Figure S6. Plots of NO_x conversion as a function of reaction time over CuO-TiO_2 NTs and CuO-TiO_2 NPs in the presence of SO_2. Reaction conditions: 270 °C, 500 ppm of NO, 500 ppm of NH_3, 5 vol% O_2, 100, 250, 500 ppm of SO_2, N_2 as the balance gas, and GHSV of 50,000 h^{-1}.

Note: With SO_2 concentration increasing to 250 and 500 ppm, the NO_x conversion of CuO-TiO_2 NTs decreased to 75% after introducing SO_2 for 10 h and recovered to 86% after removing SO_2 for 2 h. By comparison, the NO_x conversion of CuO-TiO_2 NPs decreased to 39% after introducing SO_2 for 10 h and almost unchanged after removing SO_2 for 2 h.

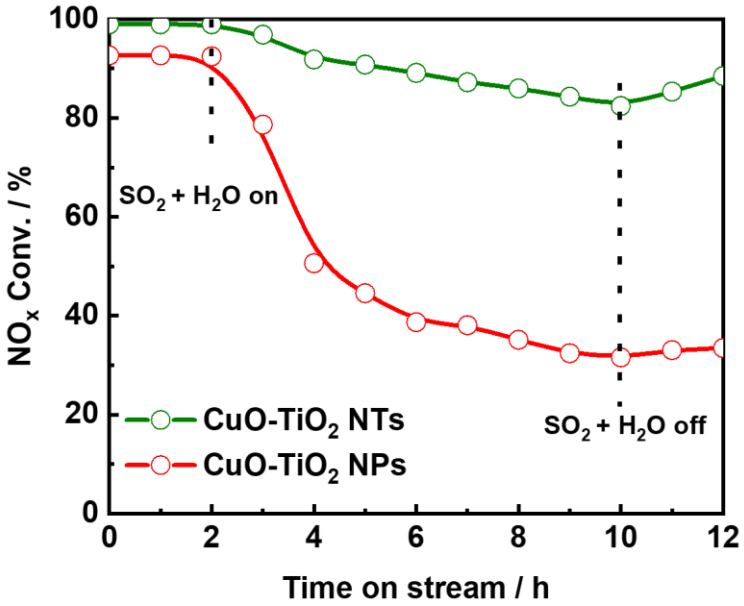

Figure S7. Plots of NO_x conversion as a function of reaction time over CuO-TiO_2 NTs and CuO-TiO_2 NPs in the presence of SO_2 and H_2O. Reaction conditions: 270 °C, 500 ppm of NO, 500 ppm of NH_3, 5 vol% O_2, 5 vol% H_2O, 100 ppm of SO_2, N_2 as the balance gas, and GHSV of 50,000 h^{-1}.

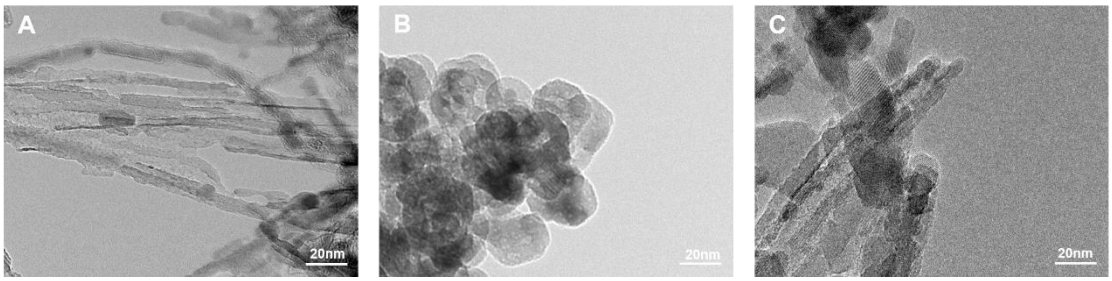

Figure S8. TEM images of (A) CuO-TiO_2 NTs, (B) CuO-TiO_2 NPs and (C) CuO-out-TiO_2 NTs.

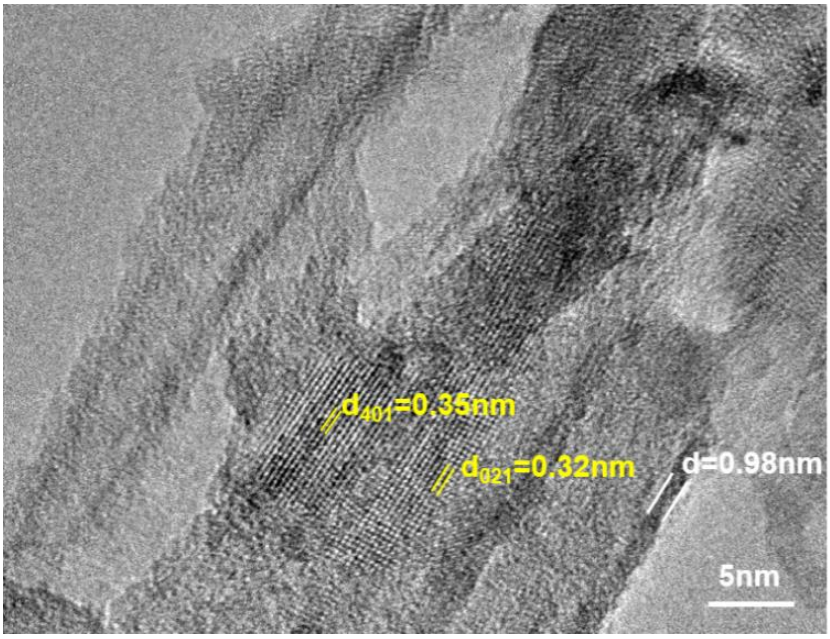

Figure S9. HRTEM image of CuO-TiO_2 NTs.

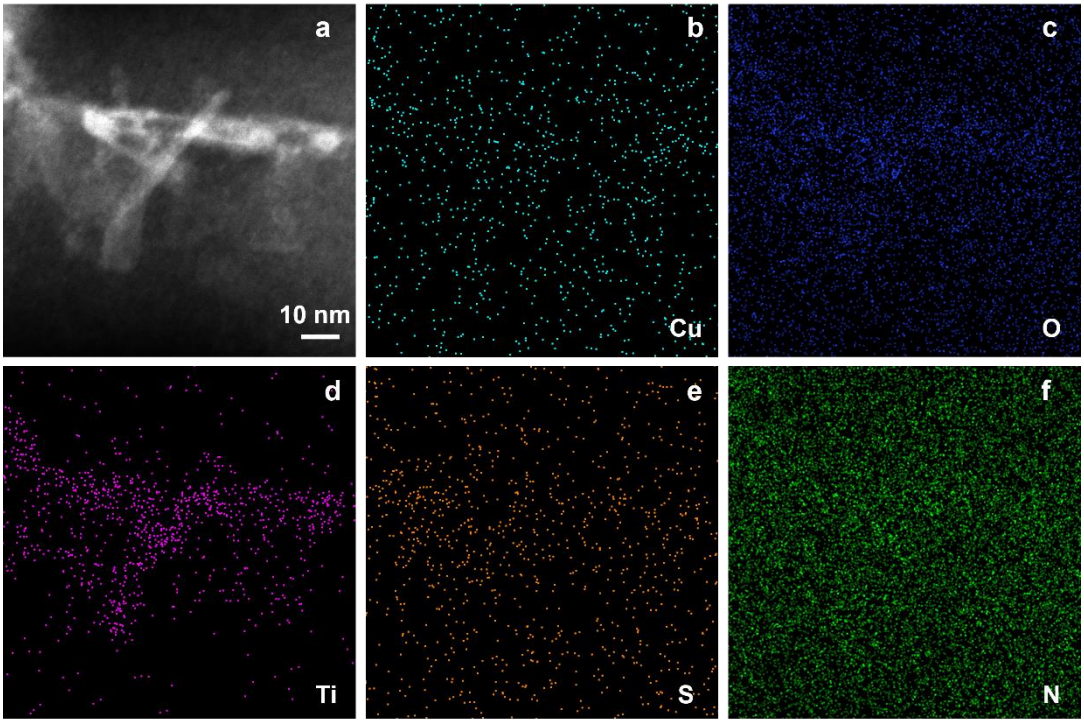

Figure S10. (a) STEM image and EDX mapping results of (b) Cu, (c) O, (d) Ti, (e) S, (f) N elements distribution for the CuO-TiO_2 NTs (s).

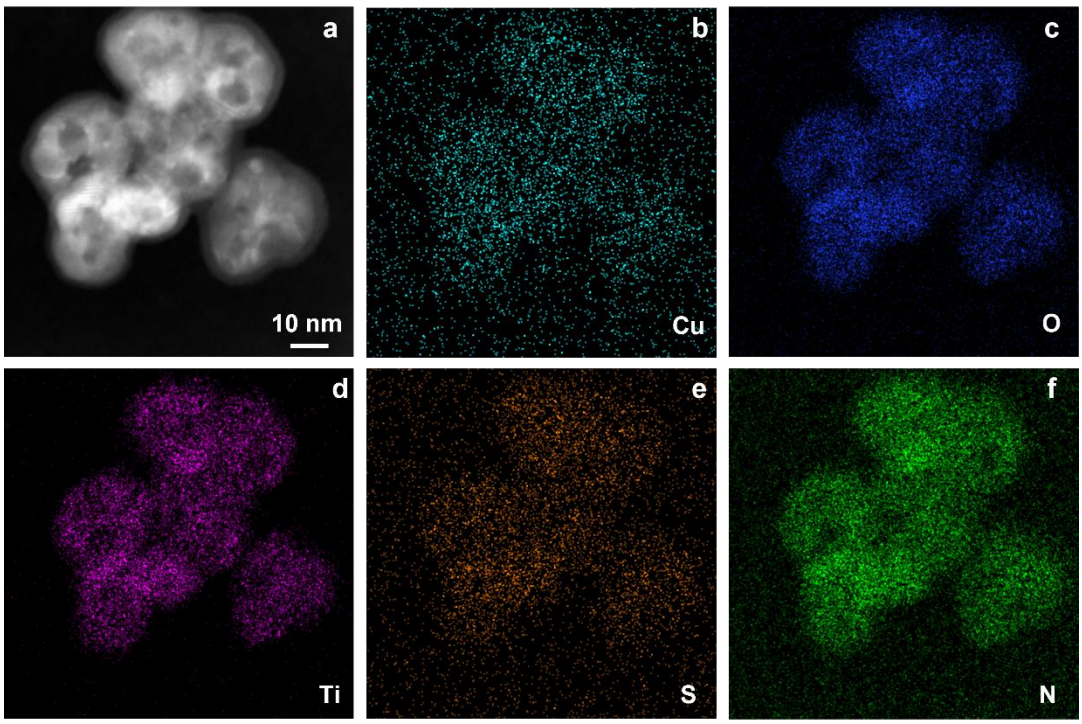

Figure S11. (a) STEM image and EDX mapping results of (b) Cu, (c) O, (d) Ti, (e) S, (f) N elements distribution for the CuO-TiO_2 NPs (s).

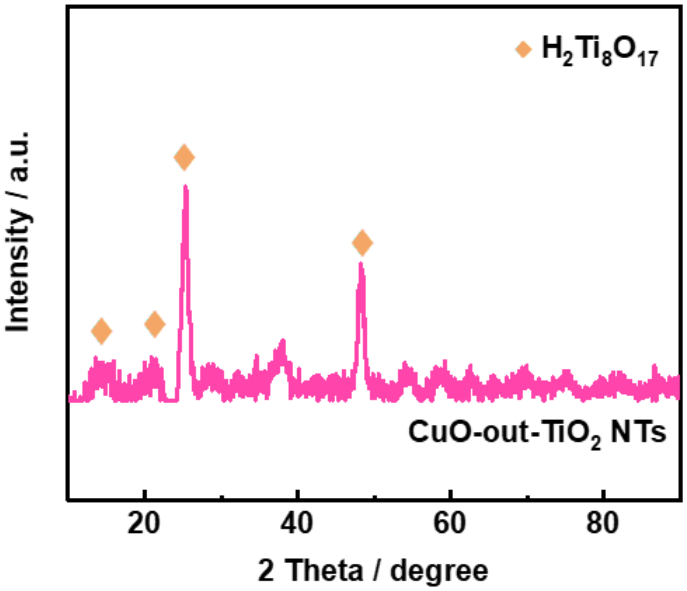

Figure S12. XRD patterns of CuO-out-TiO_2 NTs.

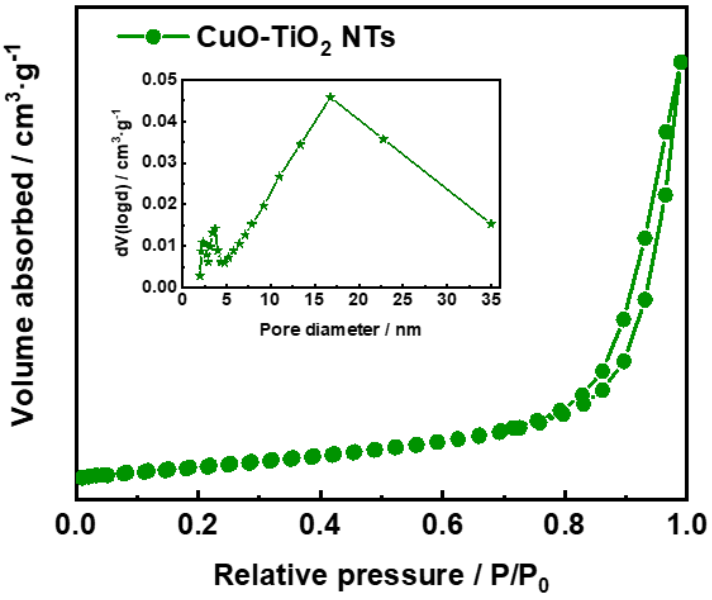

Figure S13. N_2 adsorption-desorption isotherm and BJH mesopore size distribution profiles (inset) of CuO-TiO_2 NTs.

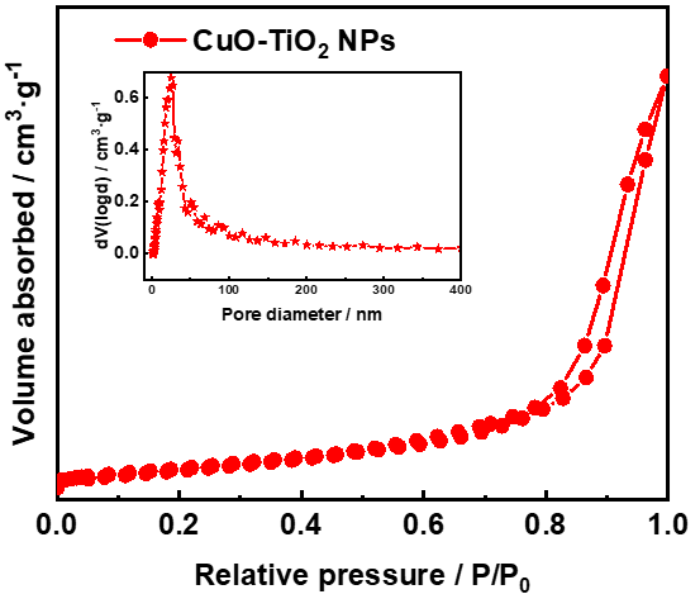

Figure S14. N_2 adsorption-desorption isotherm and BJH mesopore size distribution profiles (inset) of CuO-TiO_2 NPs.

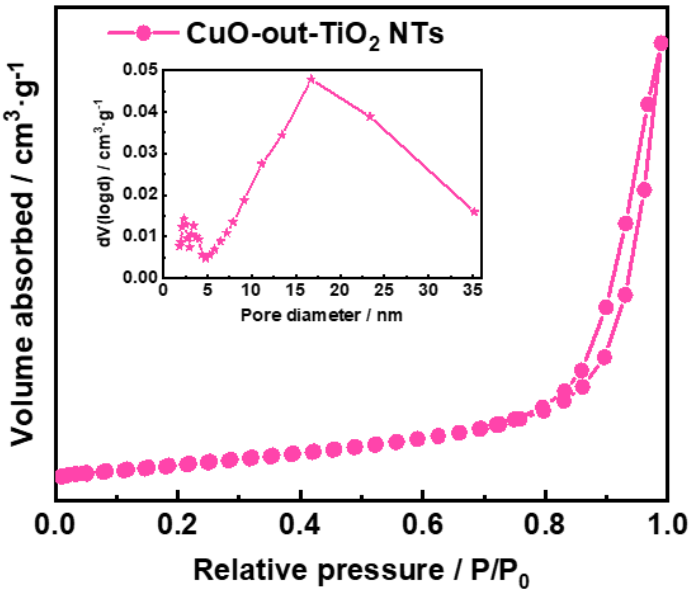

Figure S15. N_2 adsorption-desorption isotherm and BJH mesopore size distribution profiles (inset) of CuO-out-TiO_2 NTs.

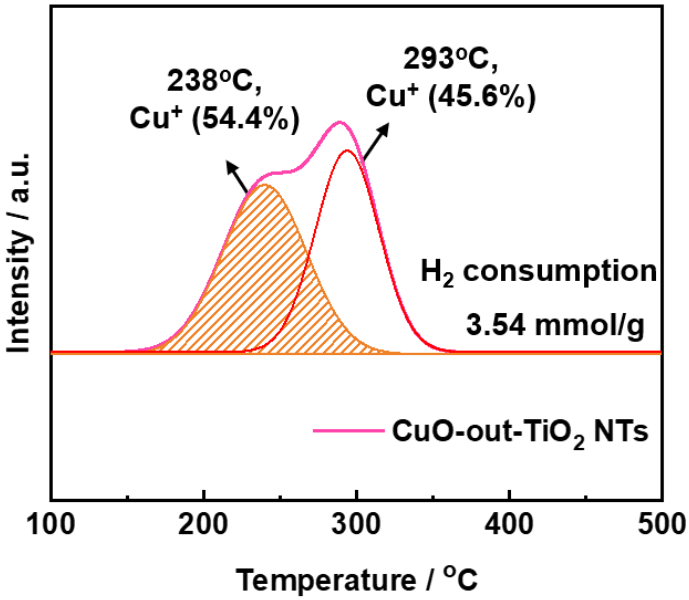

Figure S16. H_2-TPR profile of CuO-out-TiO_2 NTs.

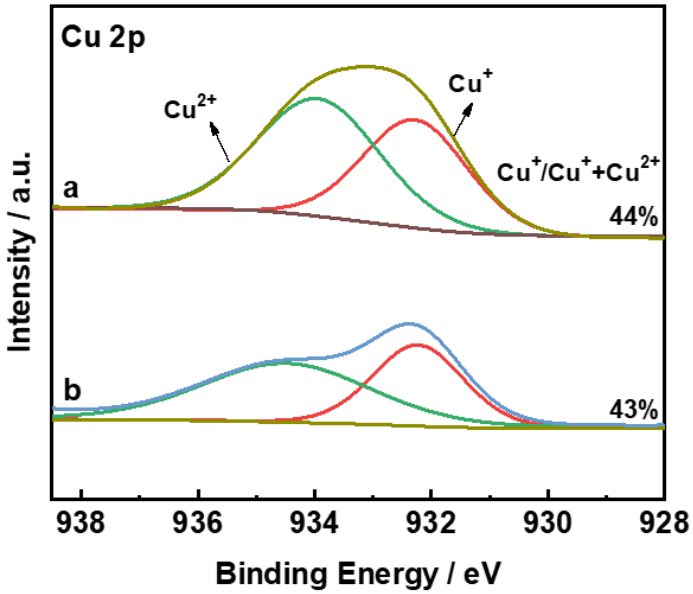

Figure S17. XPS spectra of Cu 2p over (a) CuO-out-TiO_2 NTs and (b) CuO-out-TiO_2 NTs (s).

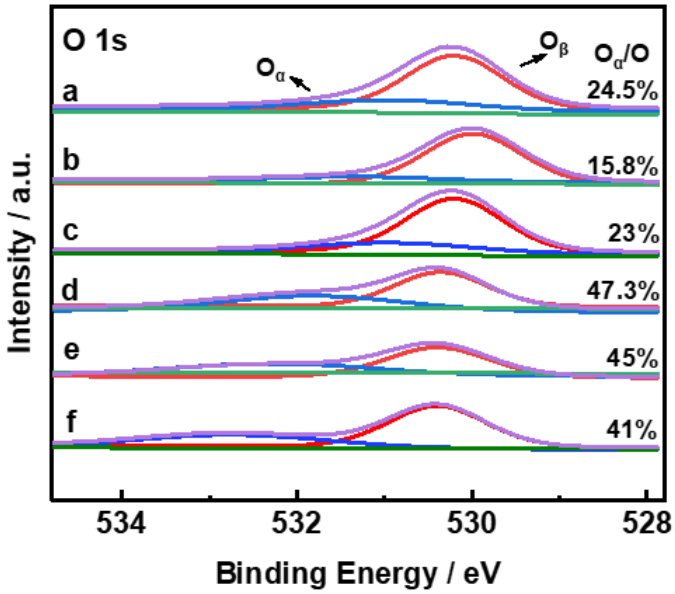

Figure S18. XPS spectra of O 1s over (a) CuO-TiO_2 NTs, (b) CuO-TiO_2 NPs, (c) CuO-out-TiO_2 NTs, (d) CuO-TiO_2 NTs (s), (e) CuO-TiO_2 NPs (s) and (f) CuO-out-TiO_2 NTs (s).

Note: In regard of the increase of $O_\alpha/O_\alpha+O_\beta$ for CuO-out-TiO_2 NTs (s) was slightly less than that of CuO-TiO_2 NTs (s), one reasonable explanation was that the penetration depth of XPS is about 2-3 nm, which can detect oxygen containing species in the tubes. Owing to the sulfates species mainly deposited outside CuO-out-TiO_2 NTs (s), for CuO-out-TiO NTs (s), it could be liable that the oxygen derived from the formed sulfates species in the tubes were lower than that of CuO-TiO_2 NTs (s).

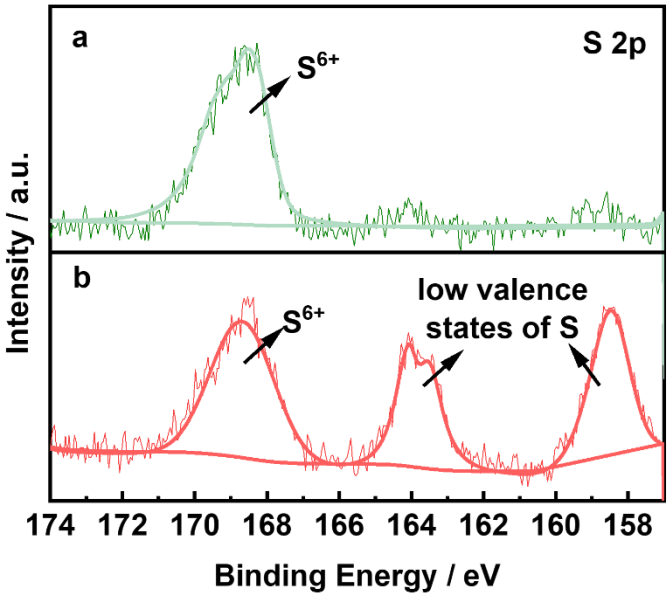

Figure S19. XPS spectra of S 2p over (a) CuO-TiO_2 NTs (s) and (b) CuO-TiO_2 NPs (s) catalysts.

Note: The peaks of binding energy at 166.0-171.0 eV were ascribed to S^{6+} which derived from SO_4^{2-}. Additionally, the peaks of binding energy at 157.0-161.0 eV and 161.0-166.0 eV were ascribed to the low valence state of S which generated by the high-energy electron bombard abundant S on the surface of CuO-TiO_2 NPs (s). [7] Owing to the quantity of sulfates species deposited on the surface of CuO-TiO_2 NPs (s) was much more than that of CuO-TiO_2 NTs (s), it would lead the surface sulfates to be more prone to facilitate the low valence state of S under the XPS electron bombardment.

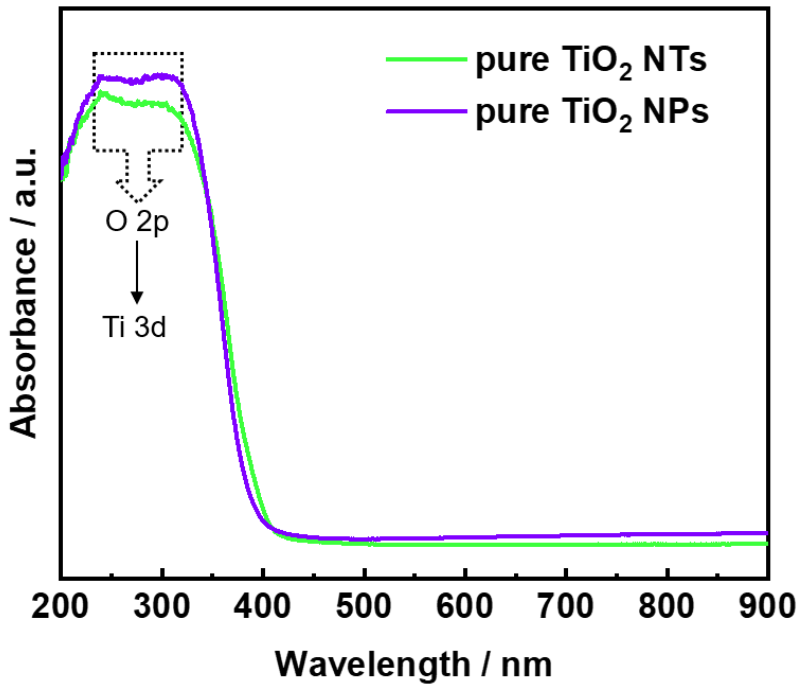

Figure S20. UV-vis absorption spectra of pure TiO_2 NTs and pure TiO_2 NPs.

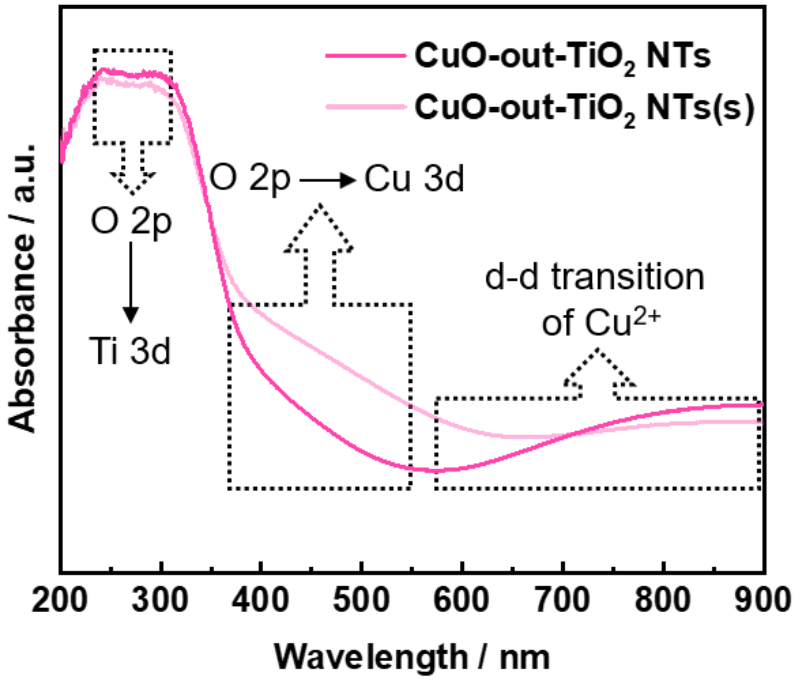

Figure S21. UV-vis absorption spectra of CuO-out-TiO_2 NTs and CuO-out-TiO_2 NTs (s).

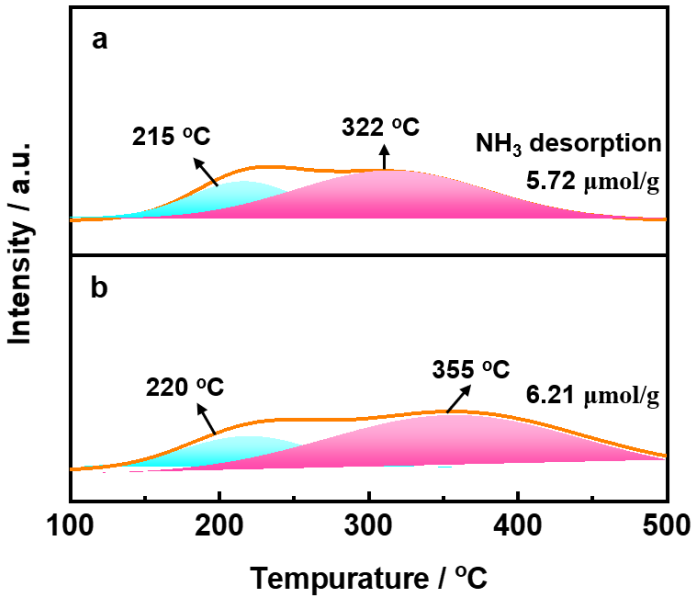

Figure S22. NH_3-TPD-MS profiles of (a) pure TiO_2 NTs and (b) pure TiO_2 NPs.

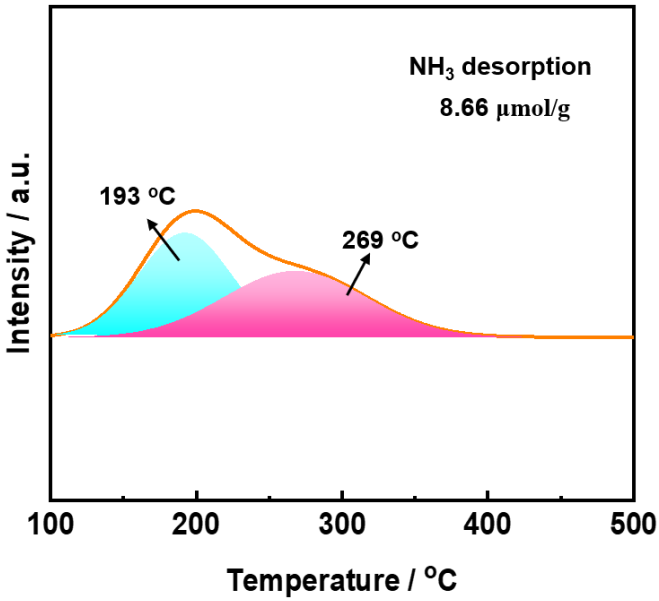

Figure S23. NH_3-TPD-MS profiles of CuO-out-TiO_2 NTs.

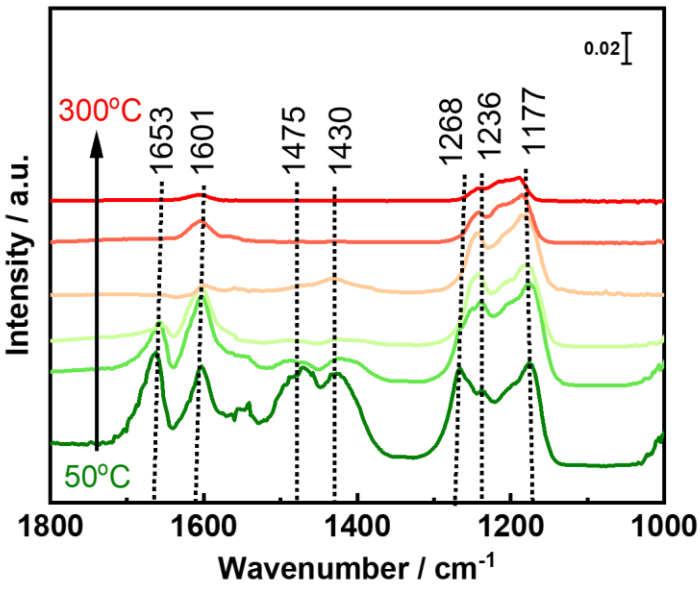

Figure S24. *In situ* DRIFTS of NH_3 desorption after 1000 ppm NH_3 pre-adsorbed for 1 h as a function of temperature over CuO-out-TiO_2 NTs.

Note: The peaks appearing at 1653 cm^{-1}, 1475 cm^{-1} and 1430 cm^{-1} were attributed to the symmetric bending vibrations of N-H for the NH_4^+ on Brønsted acid sites. Otherwise, the bands at 1601 cm^{-1}, 1268 cm^{-1}, 1236 cm^{-1}, and 1177 cm^{-1} were attributed to NH_3 on Lewis acid sites. [8-10]

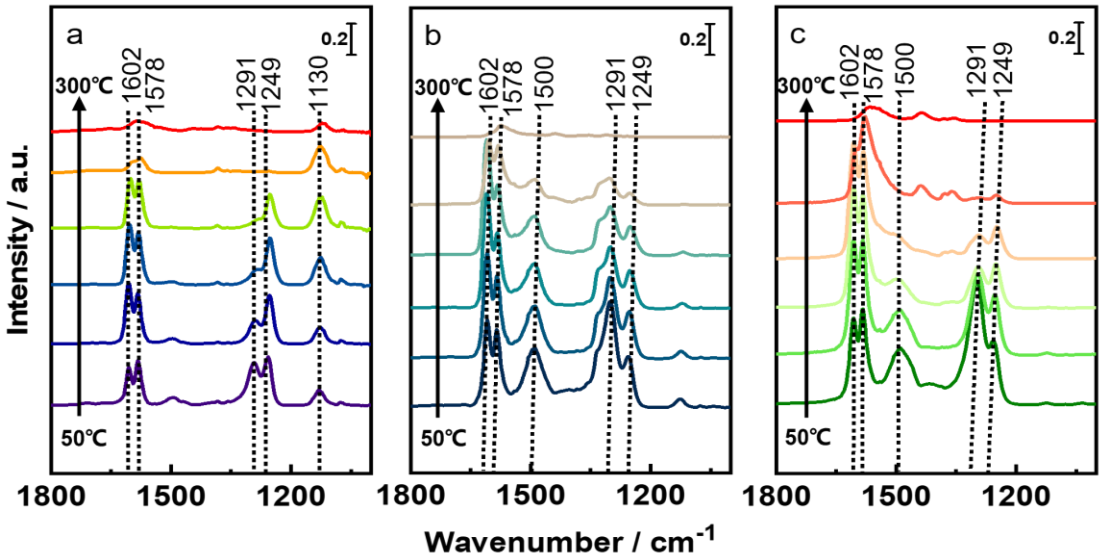

Figure S25. *In situ* DRIFTS of NO + O_2 desorption after 1000 ppm NO + 5 vol% O_2 pre-adsorbed for 1 h as a function of temperature over (a) CuO-TiO_2 NTs, (b) CuO-TiO_2 NPs and (c) CuO-out-TiO_2 NTs.

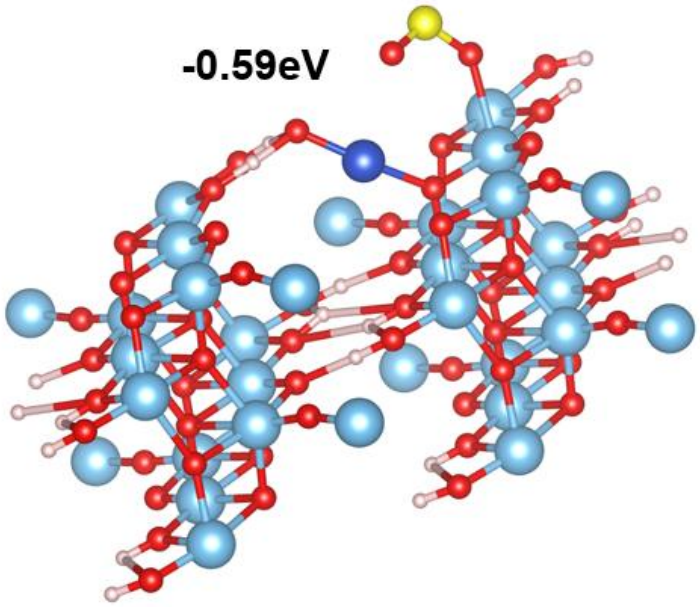

Figure S26. The most stable adsorption configuration for SO_2 adsorbed on the $H_2Ti_3O_7$ (110) sites on the CuO-TiO_2 NTs surface. Red, yellow, light blue, dark blue and white balls denote O, S, Ti, Cu and H atoms, respectively.

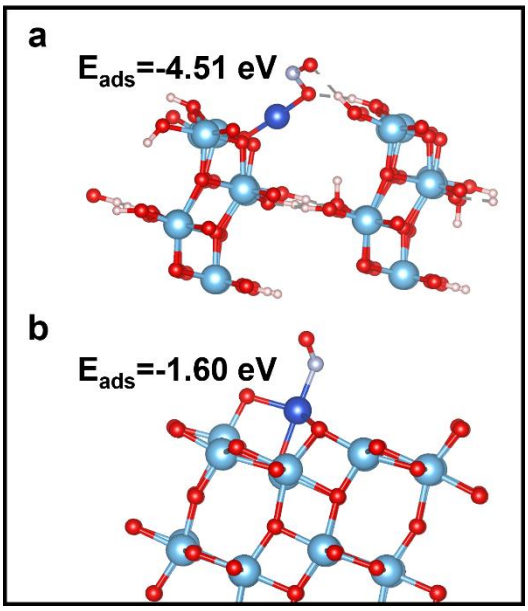

Figure S27. The most stable adsorption configuration for NO on isolated (a) CuO-TiO_2 NTs and (b) CuO-TiO_2 NPs surfaces. Grey, Red, light blue, dark blue and white balls denote N, O, Ti, Cu and H atoms, respectively.

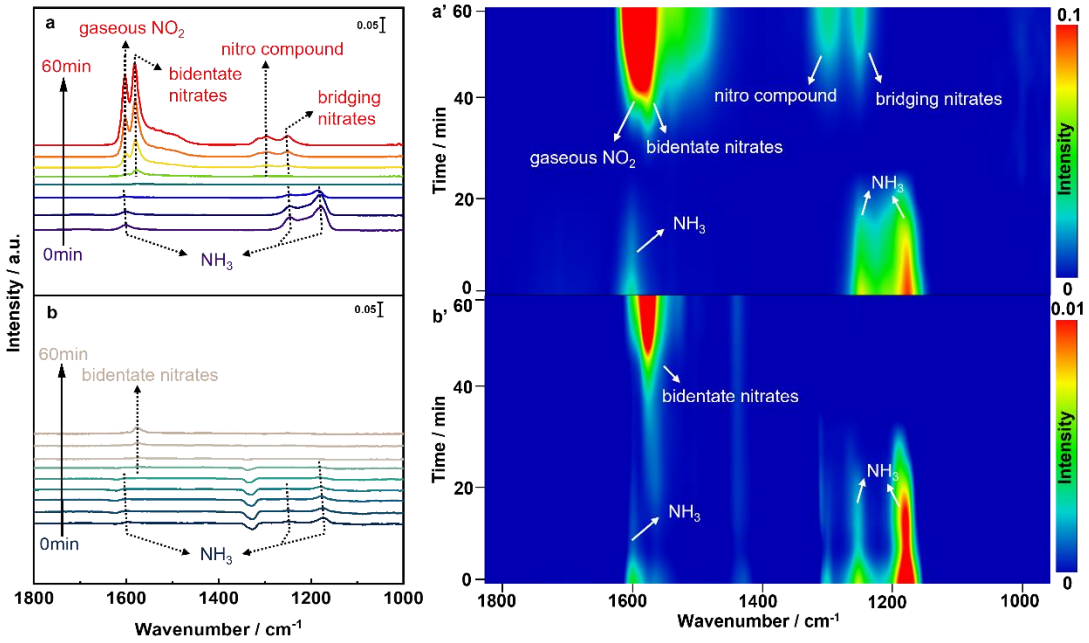

Figure S28. *In situ* DRIFTS and the corresponding mapping results of the transient reactions at 200 °C between 1000 ppm NO + 5 vol% O_2 and pre-adsorbed 1000 ppm NH_3 for 1 h as a function of time over (a, a') CuO-TiO_2 NTs and (b, b') CuO-TiO_2 NPs. Note: For the CuO-TiO_2 NTs, after the pre-adsorption of 1000 ppm NH_3 for 1 h, the band at 1180 cm^{-1} was attributed to the asymmetric bending vibration of the N-H bond of NH_3 on the Lewis site. The bands presented at 1245 cm^{-1} and 1601 cm^{-1} were also associated with NH_3 on Lewis acid sites. [11, 12] With 1000 ppm NO + 5 vol% O_2 were introduced, the NH_3 on Lewis acid sites was gradually depleted within 30 min. In addition, the bands at 1602 cm^{-1}, 1578 cm^{-1}, 1293 cm^{-1} and 1249 cm^{-1} corresponded to gaseous NO_2, bidentate nitrates, nitro compound and bridging species emerged, respectively. [8] The peak intensity of all adsorbed species gradually enhanced with the NO + O_2 introducing. In contrast, after the pre-adsorption of 1000 ppm NH_3 for 1 h, the quite weak bands at 1599 cm^{-1}, 1250 cm^{-1} and 1176 cm^{-1} also corresponded to NH_3 on

Lewis acid sites appeared over the CuO-TiO_2 NPs catalyst, which further declared the weaker surface acidity and NH_3 adsorption on CuO-TiO_2 NPs. With the introduction of 1000 ppm NO + 5 vol% O_2, the weak adsorbed NH_3 on Lewis acid sites vanished, with the weak peak at 1578 cm^{-1} which belonged to split V_3 vibrations of bidentate nitrates was apparent gradually. [13]

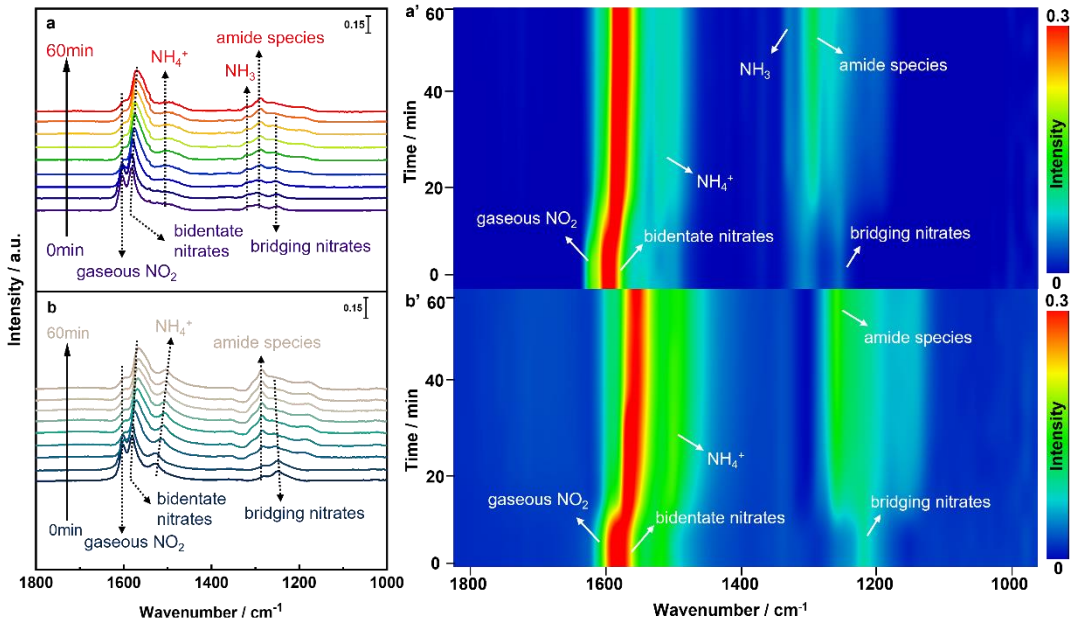

Figure S29. *In situ* DRIFTS and the corresponding mapping results of the transient reactions at 200 °C between 1000 ppm NH_3 and pre-adsorbed 1000 ppm NO + 5 vol% O_2 for 1 h as a function of time over (a, a') CuO-TiO_2 NTs and (b, b') CuO-TiO_2 NPs.

Table S1. The atomic fraction of N, S and Cu of CuO-TiO_2 NTs (s) and CuO-TiO_2 NPs (s) obtained from TEM-EDX mapping.

Sample	Atomic fraction of S (%)	Atomic fraction of N (%)	Atomic fraction of Cu (%)
CuO-TiO_2 NTs (s)	3.63	8.19	4.24
CuO-TiO_2 NPs (s)	5.70	8.39	4.99

Table S2. The textural properties of $CuO\text{-}TiO_2$ NTs, $CuO\text{-}TiO_2$ NPs, $CuO\text{-out-}TiO_2$ NTs, $CuO\text{-}TiO_2$ NTs (s), $CuO\text{-}TiO_2$ NPs (s) and $CuO\text{-out-}TiO_2$ NTs (s).

Catalysts	Specific surface area ($m^2 \cdot g^{-1}$)	Pore volume ($cm^3 \cdot g^{-1}$)
$CuO\text{-}TiO_2$ NTs	270.6	1.51
$CuO\text{-}TiO_2$ NPs	68.0	0.39
$CuO\text{-out-}TiO_2$ NTs	286.8	1.57
$CuO\text{-}TiO_2$ NTs (s)	181.8	0.41
$CuO\text{-}TiO_2$ NPs (s)	76.4	0.25
$CuO\text{-out-}TiO_2$ NTs (s)	124.5	0.38

Table S3. The hydrogen consumption and the ratios of hydrogen consumption from different Cu reduction peaks of CuO-TiO_2 NTs, CuO-TiO_2 NPs and CuO-out-TiO_2 NTs.

Sample	Hydrogen consumption of Cu^+ reduction (%)	Hydrogen consumption of Cu^{2+} reduction (%)	Total hydrogen consumption (mmol/g)
CuO-TiO_2 NTs	67.2	32.8	3.62
CuO-TiO_2 NPs	49.2	50.8	2.07
CuO-out-TiO_2 NTs	45.6	54.4	3.54

Table S4. The atomic fraction of N and S of CuO-TiO_2 NTs (s) and CuO-TiO_2 NPs (s) catalysts obtained from XPS measurement.

Sample	Atomic fraction of N (%)	Atomic fraction of S (%)
CuO-TiO_2 NTs (s)	3.16	3.65
CuO-TiO_2 NPs (s)	2.84	6.17

Note: The atomic fraction of S on the surface of CuO-TiO_2 NPs (s) was 6.17%, much higher than that (3.65%) of CuO-TiO_2 NTs (s), which indicated that there were more sulfates species yielded on the surface of CuO-TiO_2 NPs (s) than that of CuO-TiO_2 NTs (s). Meanwhile, the atomic fraction of S on the surface of CuO-TiO_2 NTs (s) was about the same as the atomic fraction of N (3.16%). It indicated that most of sulfates species deposited on the surface of CuO-TiO_2 NTs (s) in the form of $(NH_4)_2SO_4/NH_4HSO_4$ species rather than $CuSO_4$, which would decompose at lower temperature and express less poisoning effects on the catalyst activity. In contrast, the adsorption of SO_2 on the surface of CuO-TiO_2 NPs (s) generated more $CuSO_4$ species beyond that $(NH_4)_2SO_4/NH_4HSO_4$, resulting in serious active sites poisoning and activity loss.

Table S5. The mass fraction of S among CuO-TiO_2 NTs (s) and CuO-TiO_2 NPs (s) obtained from ICP measurement.

Sample	Mass fraction of S (%)
CuO-TiO_2 NTs (s)	2.47
CuO-TiO_2 NPs (s)	3.47

Table S6. The NH_3 desorption amount and the ratio of ammonia desorption on different acid sites of CuO-TiO_2 NTs, CuO-TiO_2 NPs, CuO-out-TiO_2 NTs, pure NTs and pure NPs.

Sample	Weak NH_3 desorption (0~200 ºC, %)	Medium-strong NH_3 desorption (>200 ºC, %)	Total NH_3 desorption (μmol/g)
CuO-TiO_2 NTs	38.3	61.7	14.39
CuO-TiO_2 NPs	34.6	65.4	10.88
CuO-out-TiO_2 NTs	50.0	50.0	8.66
Pure NTs	32.0	68.0	5.72
Pure NPs	28.8	71.2	6.21

References

1. G. Kresse and J. Furthmüller, Efficient iterative schemes for ab initio total-energy calculations using a plane-wave basis set, *Phys. Rev. B*, 1996, **54**, 11169-11186.
2. G. Kresse and D. Joubert, From ultrasoft pseudopotentials to the projector augmented-wave method, *Phys. Rev. B*,1999, **59**, 1758.
3. J. P. Perdew, K. Burke and M. Ernzerhof, Generalized gradient approximation made simple, *Phys. Rev. Lett.*,1996, **77**, 3865.
4. S. Grimme, J. Antony, S. Ehrlich and H. Krieg, A consistent and accurate ab initio parametrization of density functional dispersion correction (DFT-D) for the 94 elements H-Pu, *J. Chem. Phys.*, 2010, **132**, 154104.
5. H. J. Monkhorst and J. D. Pack, Special points for brillouin-zone integrations, *Phys. Rev. B*, 1976, **13**, 5188.
6. S. Dudarev, G. Botton, S. Savrasov, C. Humphreys and A. Sutton, Electron-energy-loss spectra and the structural stability of nickel oxide: an LSDA+ U study, *Phys. Rev. B*, 1998, **57**, 1505.
7. R. Zhang, C. Sun, J. Kou, H. Zhao, D. Wei and Y. Xing, Enhancing the Leaching of Chalcopyrite Using Acidithiobacillus ferrooxidans under the Induction of Surfactant Triton X-100, *Minerals*, 2019, **9**, 11.
8. H. Hu, S. Cai, H. Li, L. Huang, L. Shi and D. Zhang, In situ DRIFTs investigation of the low-temperature reaction mechanism over Mn-doped Co_3O_4 for the selective catalytic reduction of NO_x with NH_3, *J Phys. Chem. C*, 2015, **119**, 22924-22933.
9. L. Chen, Z. Si, X. Wu and D. Weng, DRIFT study of CuO-CeO_2-TiO_2 mixed oxides for NO_x reduction with NH_3 at low temperatures, *ACS Appl. Mater. Interfaces*, 2014, **6**, 8134-8145.
10. K. Zha, S. Cai, H. Hu, H. Li, T. Yan, L. Shi and D. Zhang, In situ DRIFTs investigation of promotional effects of tungsten on MnO_x-CeO_2/meso-TiO_2 catalysts for NO_x reduction, *J Phys. Chem. C*, 2017, **12**, 25243-25254.
11. Q. Zhang, J. Fan, P. Ning, Z. Song, X. Liu, L. Wang, J. Wang, H. Wang and K. Long, In situ DRIFTS investigation of NH_3-SCR reaction over CeO_2/zirconium phosphate catalyst, *Appl. Surf. Sci.*, 2018, **435**, 1037-1045.
12. H. Liang, K. Gui and X. Zha, DRIFTS study of γFe_2O_3 nano-catalyst for low-temperature selective catalytic reduction of NO_x with NH_3, *Can. J. Chem. Eng.*, 2018, **94**, 1668-1675.
13. H. Hu, S. Cai, H. Li, L. Huang, L. Shi and D. Zhang, Mechanistic aspects of deNO_x processing over TiO_2 supported Co-Mn oxide catalysts: structure-activity relationships and in situ DRIFTs analysis, *ACS Catal.*, 2015, **5**, 6069-6077.